
Politecnico di Torino

Department of Control and Computer Engineering

Master Course in Mechatronic Engineering

# Design of a haptic interface using induction actuators

***Academic advisor***
Prof. Massimo CANALE

***External Advisor***
**ISIR-Sorbonne University**
Dr. Sinan HALIYO
Ing. GeorgeDAHER

*Presented by:*
Ali HAMMOUD

## List of Figures

## List of Tables

# TABLE OF CONTENTS

# Chapter 1
# Introduction

Due to recent advances in micro-technologies and increasing demand for new micro-systems for fields like micro-manufacturing, medicine, biotechnology, characterization of new material, etc., micro-robotics have emerged enabling access to these micro-environments, since macro-scale robots and human operators cannot interact directly and access such tiny spaces. In addition, micro-scale physics differs completely from that of our perceptible macro-scale. Fully automated systems and manual operations limit the possibilities and hamper the ease of carrying out tasks. The use of haptic feedback tele-operation seems to be a promising solution as it allows high flexibility and improved intuitiveness. Thus, taking advantage of the precision of the machine and the perfection of the dexterity of the human operator. This approach, however, is full of challenges:
• Communication between the haptic interface and the slave micro-manipulator should be well established without any latency or loss of information.
• The haptic interface should be designed to meet human haptic perception and to faithfully render to the operator the highly dynamic phenomenon and the large bandwidth of force present at the micro-scale.
The main goal of this work is to overcome these challenges by designing high fidelity haptic interfaces coupled to a slave micro-manipulator to perform micro-assembly tasks. This work is part of an ANR project called COLAMIR, whose main objective is to show that collaborative robotics is the key to improve micro-manufacturing.
The thesis is focusing on linear induction motor design to be used in haptic interface.
The main concerns of this study is:

- The shape of the traveling magnetic field in the air gap of the DSLIM, which has the most critical influence on the smoothness and the quality of the force. The shape of the traveling magnetic field is mainly affected by the winding design of the motor, its number of phases, and the form of the control input signal applied to it.
- In order to understand the behavior of the motor , a deep study have been done starting from modeling the system taking into consideration of all parameters including the tilt between the primary and the secondary of the motor which is usually neglected due to the linear motion of secondary with respect to the primary.

The thesis is structured as follows:
The first chapter describes the principle of operation of the motor with its theories. The second chapter presents an impressive way to improve the shape of

the magnetic field without further complicating its winding design and manufacturing process by offsetting one of its primary to the other.The third chapter is mostly about the DSLIM equations that should be used in order to simulate the generated force by DSLIM.The fourth chapter is focusing on the steps done to implement the tilt in force equation.In the fifth chapter an equivalent circuit have been modeled in order to study the effect of all inputs on the motor generation in the sixth chapter.After identifying inputs that can effect force generation in haptic interface case system Identification is done in the the seventh chapter.

# Chapter 2
# State of Art

## 2.1 Introduction

Direct human manipulation of relatively small objects is not an easy task. The user must be well trained to perform these kind of tasks that are for most of the time exhausting and time consuming. The smaller the objects the harder the task as microscale is not accessible directly by human. In addition, physics at micro and nano scales are different from that of our scale. In microscale, surface tensions are predominant, the mobility is better and the dynamics is higher [1]. Precise and accurate robots are needed in order to access the microscale, but the complexity lies in controlling the robot to perform the task because the information collected by the microscope alone is not enough to manipulate and predict what might happen during themanipulation of micro-objects where adhesion and surface forces are not negligible.

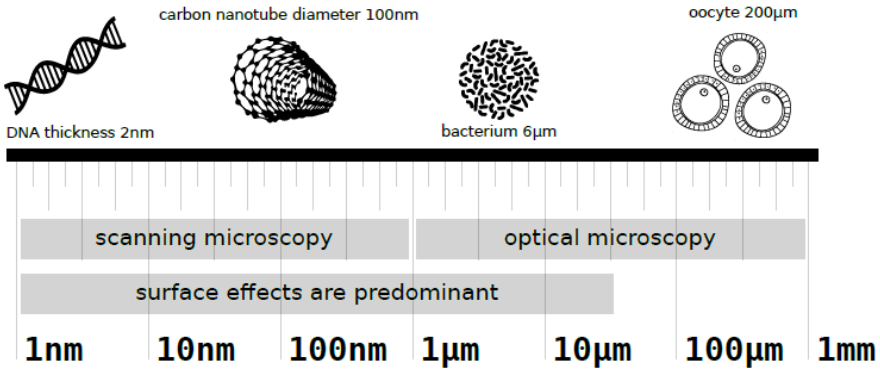


Figure 1: size comparison micro and nano scale

Sensing at micro-scale become so incredibly important because of the uncertainties, sensing will enable us to: detect the state and shape ofmicro-objects, determine their position and orientation, handle of fragile samples, verify the quality of links, control a task realization, close the loop for control, measure the mechanical properties of the sample, explore and investigate objects. (FIGURE 2). shows some examples of micro force sensors. Fully automated robotic assembly approach requires a fully pre-determined task. To solve this problem, the use of haptic feedback teleoperation seems to be a promising solution as it allows high flexibility and intuitiveness [2]. Thus, by merging both human and machine capabilities to perform the task we take advantage of the precision

of the machine and the perfection of the dexterity of the human operator. By transferring the desired actions of the operator to the executing machine and by transmitting sensory information from the micro world, measured by sensors embedded in the manipulating slave robot and rendered by the haptic interface, to the operator (FIGURE 3).

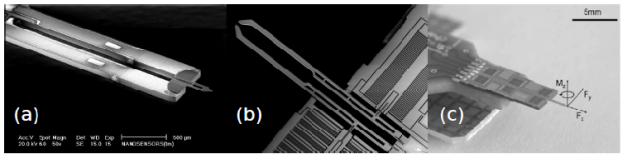


Figure 2: (a) SEM image of Akiyama self sensing AFM Probe based on a quartz tuning fork combined with a micromachined cantilever, (b) SEM image of Femtotools FT-G Microgripper designed to handle objects ranging from0.001mmto 0.1mmwith an integrated force sensor for gripping force measurement, (c) micro force-torque sensor that can measure simultaneously two force components Fx, Fy and a torque component Mz [3]

## 2.2 Haptic interfaces and teleoperation chains

Teleoperation is a unique way of overcoming the limitations of sensory perception and human manipulation. Teleoperation refers to the use of two systems, designated as master (Haptic interface) and slave (distant robot). These systems are coupled to transfer in real time the efforts and actions. These techniques are used to create access to systems naturally inaccessible by their scales, or distances. [4, 5, 6].

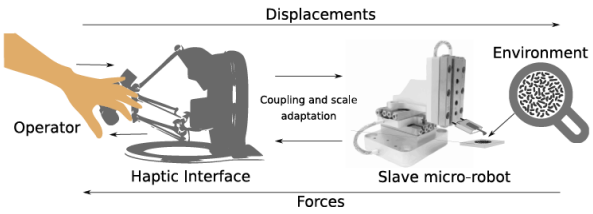


Figure 3: Bilateral microteleoperation, Haptic interaction with a micro environment

The human operator closes the control loop of a teleoperated system, since in haptic perception the flow of energy is bidirectional, unlike other senses. In addition, touch sensations are very sensitive to vibrations [7], able to detect very small displacements and faster than the sense of vision [8]. Given the following facts, more "realism" and "presence" occur during the execution of the task, thus increasing its quality. The capacity in terms of autonomy of the executing machine greatly influences the nature of the human-machine interaction and the control-command strategies. The sense of touch delivers rich and detailed information about an object and when combined with other senses, especially sight, touch dramatically increases the amount of information sent to the brain for processing. The increase in information reduces the time to complete a task, as well as user error. It also reduces the energy consumption and the magnitudes of contact forces used in a teleoperation situation. Teleoperationwith haptic feedback is one solution to transmit information intuitively to operators. [5]. Teleoperation composed of both haptic and visual feedback of the scene enables non expert users to performcomplex teleoperatedmicromanipulation tasks.

## 2.3 Human haptic perception

Knowledge gained on human haptic perception helped to understand howto develop and improve the design of haptic interfaces. Increasing the synergy between the human operator and the interface increases the quality of the performed task by ensuring very good exchange of information. The human haptic perception relates to two cognitive senses the tactile sense and the kinesthetic sense and both are very important for to manipulation and locomotion [9, 10, 11].

• Tactile sense: The tactile sense refers to perceptions of texture, pressure, vibration and temperature, it is related to tactile mechanical receptors located at the level of the skin [12]. Tactile sensations are usually stimulated by vibrations. For instance, at the finger level, where the discrimination resolution is high, frequencies up to 1 KHz with 1 mdisplacement can be detected [13].

• Kinesthetic sense: The kinesthetic sense refers to the perception of the body in space and muscular effort through receptors located in the muscles, tendons, skin and joints [14]. The kinesthetic sense is usually stimulated by exercising a force feedback to the user to recreate an object.

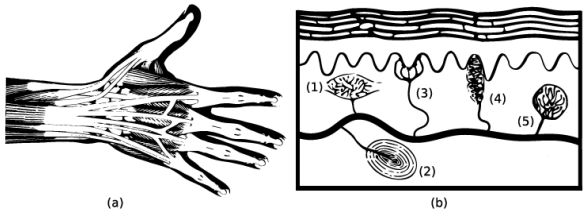


Figure 4: (a) Human handmuscles and tendons, (b) schematic section of a human skin (1) Ruffini's ending (pressure), (2) Pacianian corpuscule (pressure), (3) Merkel disks (touch), (4) Meissner's corpuscle (touch), (5) Krause's copuscle (cold receptor)

These two senses are generally addressed and treated separately, that's why there are typically two types of HIs; tactile interfaces and kinesthetic interfaces. And since both stimuli are important and essential for human perception, this division is neither intuitive nor effective. In recent years, given the importance of simultaneously stimulating both tactile and kinesthetic senses, HIs that activate both senses started to appear. [15, 16, 17].

## 2.4 High fidelity haptic interface design requirements

Nowadays, the field of haptics is growing rapidly, research on haptics has increased dramatically now that, the applications of haptic interfaces are found in a large range of areas including: teleoperation, rehabilitation, education, games, arts, sciences, etc. However, the mechanical structure of most existing interfaces limits the transparency and rendering of haptic interactions. Body-based haptic devices and non-intrusive haptic interfaces with different stimulation technologies as wearable haptic devices and non-contact haptic devices offer high levels of transparency in free movement yet, they do not provide enough spacial force resolution and intensity [18]. Their inability to generate a real kinesthetic feedback is their main drawback. Interfaces without force feedback are not ideal for manipulation. Other studies and works have addressed these constraints and maximized the transparency of ground-based devices by adopting a complex mechanical design and an advanced dedicated control system to lower the intervening dynamics and friction of the device for a high fidelity transmission and rendering of absolute forces and torques. But nevertheless, the price of these ground-based interfaces is exceedingly high and their maintenance is expensive. In other works high transparency has been achieved with a simple mechanical design but the interface was limited to one rotational degree of freedom. [19]. High levels of transparency are required especiallywhen the interface is dedicated for telemicromanipulation tasks. The interface should be able to provide force feedback from the micro scale fores that arise during the assembly process without masking the perception of highly dynamic phenomena. These

information are important to the human somatosensory system to predict the circumstances of the environment for the accomplishment of the task.

### 2.4.1 Transparency

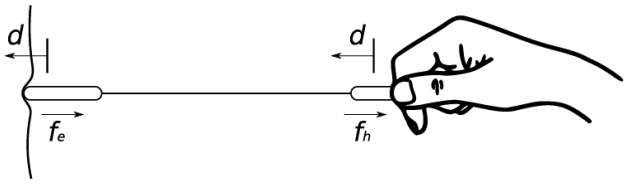


Figure 5: The idealized teleoperator. A tool having a given geometry in contact with an object is operated at a distance via the imaginary construct of a massless, infinitely rigid stick. Thiswould be equivalent to holding the tool directly [20]

The main objective of an ideal haptic device is to render the true feel of the task performed in the remote environment to the human operator. The haptic interfacemust then be able to provide an unfaltering, steady and reliable transmission of signals between the remote environment and the human operator. Ideally, when the operator's hand is free in the virtual environment the user must not feel the existence of the haptic interface, while when it encounters a virtual solid object the user movement must be blocked by the interface (the actuators must provide high forces). In recent decades, many types of haptic interfaces have been created to allow the operator to manually interact with remote systems. Over time, the quality of haptic interfaces has improved significantly thanks to the advancement of technologies in all areas: mechanical, electrical, software, etc. For example: position sensors have becomemuch more accurate in reading positions, increasing feedback resolution in control loops, thus positively affecting the accuracy and dynamics of positioning and speed control. Providing a high fidelity haptic sensation to the operator, requires a system that covers the haptic sense in human perception. The mechanical design along with the sensors, the actuator and the control systemmust be precise and quite fast in acquiring and rendering information. In short, the haptic interface must be capable of producing controllable forces that correspond to human haptic perception.

### 2.4.2 Technical and design requirements of an ideal haptic interface

An ideal haptic interface should be designed to meet human haptic perception and to faithfully render and scale forces without any distortion. The transmission of signals between the remote or virtual environment and the human operator must be unfaltered, steady and reliable. The fidelity of an haptic interface is increased by the increase of its transparency, which is obtained when

the haptic signals rendered by the device are not distracted or scrambled by itsmechanical dynamics.

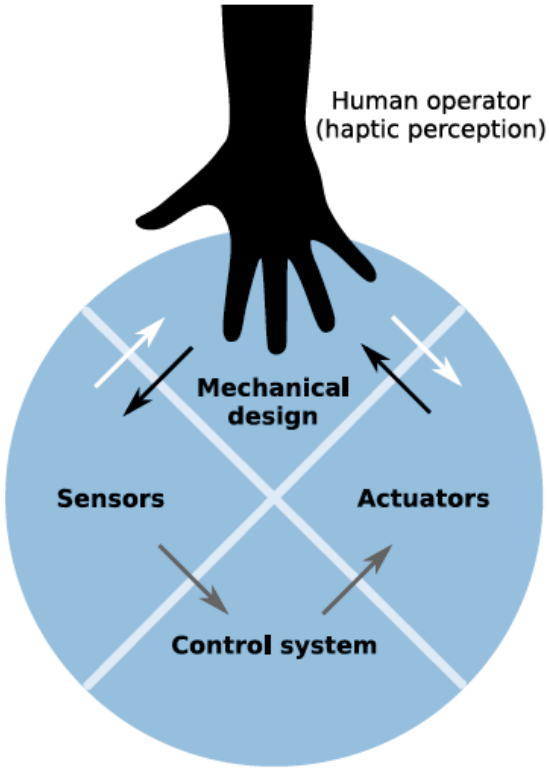


Figure 6: Robotic Haptic interface design, actuation, sensing and control to "read and write" from the human hand. The effect of the white arrows has to be minimized in the design of an haptic devise, meaning that the mechanical design must not mask the small and fine forces generated by the actuators, and reading the position of the device must not disturb its state

The choice of the actuator should be based certainly on its high performance and the sensor on its high resolution, also there integration must keep haptic distortion so small. In other words, there integration must not destruct the motion of the haptic handle by To read the state of the device many advanced tools are already in existence (lasers, fast camera, etc.) and they can measure the position without destructing the motion of the haptic handle or adding weight to it. The output of the interface, the force feedback, is in generalmore difficult to achieve. In general, haptic interfaces are selected according to the type of application and the predominant factor in this selection is the type and characteristics of its actuators. For instance, haptic devices that are able to

produce high forces will not normally be capable of producing very small and precise forces. The actuator in this case will be relatively large and massive as a result its large inertia will mask the perception of small forces. And small motors with low inertia, on the other hand, would be able to produce small and precise forces, but not large forces due to its small size. Here is a list of a set of requirements that should characterize an ideal haptic interface:

- Low Inertia
- Low Friction
- Wide Dynamic Force Range
- High Force Bandwidth
- High Structure Stiffness
- Zero Backlash
- Ergonomic
- Good Position Resolution
- Backdrivability

Its interaction with humans is what gives this device such specificities, thus a lot of attention should be dedicated to the design a such device because its demands are often discordant.

# Chapter 3
# The Double Sided Linear Induction Motor

There are mainly two types of Linear Induction Motors: the Single Sided Linear Induction Motor (SLIM) and the Double Sided Linear Induction Motor (DSLIM).

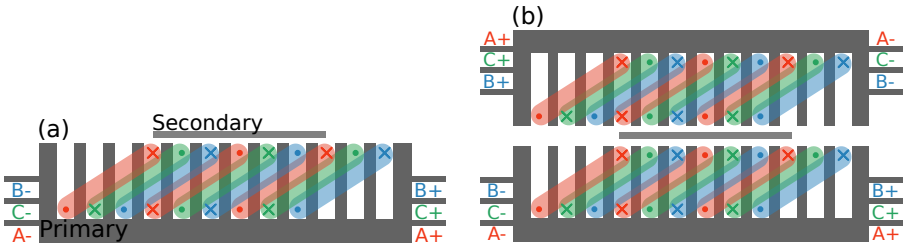


Figure 7: (a) Single Sided Linear Induction Motor, (b) Double Sided Linear Induction Motor

Compared to a Single Sided Linear Induction Motor (SLIM), the Double Sided Linear Induction Motor (DSLIM) has a higher force density, less significant end effect, and the resultant normal force on the secondary remains equal to zero.

The secondary of the motor, the moving part, can weigh a few grams, and therefore its inertia can be minimal, which is exciting for applications where the effects of weight and inertia are not desired. The low inertia of a haptic handle increases the transparency and fidelity of the interface. Its low inertia would not introduce extra undesired forces during manipulation.

## Linear Induction Motor Geometry

Table 1: Geometrical parameters

| Symbol | Description |
|---|---|
| $w_t$ | tooth width |
| $w_s$ | slot width |
| $e_{wt}$ | extremity tooth width |
| $\lambda$ | slot pitch |
| $h_s$ | slot height |
| $h_y$ | yoke height |
| $M_W$ | motor width |
| $M_L$ | motor length |
| $M_H$ | motor height |

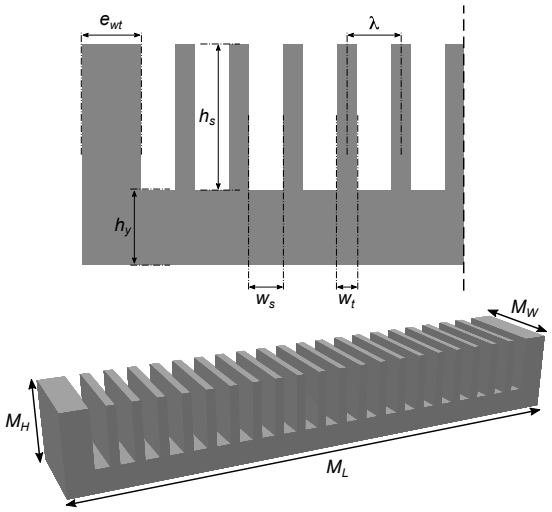


Figure 8: LIM geometry

# Chapter 4
# LIM principle of operation

When we input the primaries of the double sided linear motor with three sine waves at 120 degrees of phase shift a time-travelling magnetic field B is generated in the air gap. when it goes through the conducting material, the aluminum plate, it causes a magnetic flux $\Phi_B$ .

The change in magnetic flux induces an *emf* (Electromotive force) in the material according to Farady's law of induction.

$$\varepsilon_{induced} = -\frac{d\ \Phi_B}{dt} \tag{1}$$

The current induced in the conductive plate is given by Ohm's law, since the conductive material has some resistance $R$.

$$I_{induced} = \frac{\varepsilon_{induced}}{R} = -\frac{1}{R} \times \frac{d\ \varepsilon_{induced}}{dt} \tag{2}$$

In turn, the induced current also called Eddy current generates another magnetic field according to Ampere's law, which itself has a magnetic flux. This induced magnetic flux opposes the change in the original magnetic flux caused by the primaries of the motor. This is given by Lenz's law which states that the induced currents flow in such a way that they create a magnetic field that opposes the change that produced them. The direction of the induced current can be determined using the right-hand rule, the thumb is pointing in

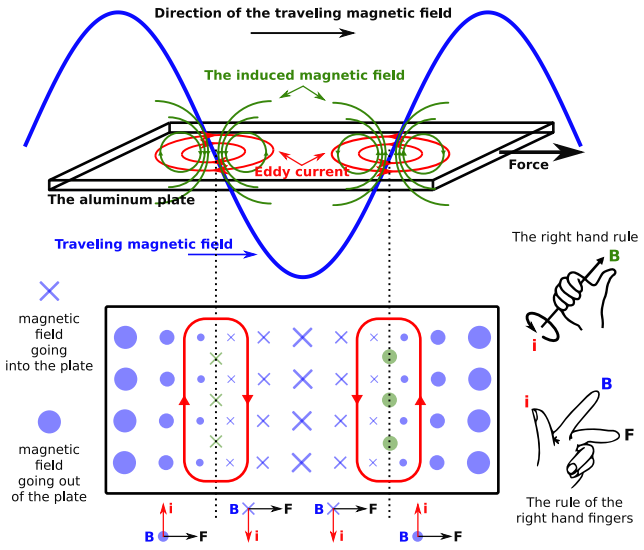


Figure 9: Principle of operation of the motor

the direction of the magnetic field generated by eddy currents, the curling of the four other fingers reveals the direction of the current. (figure 9).

The magnetic field then acts on the mobile particles, the conduction electrons, of the conductor which transmit integrally, to the structure, the resultant of Lorentz forces which they undergo. The force of Lorentz is the force that a moving particle experiences when it enters an electromagnetic field. And the consequent of the Lorentz forces exerted on the mobile charges of the moving conductor is known as the force of Laplace. The law of Laplace states that "A conductor through which current flows and placed in a magnetic field is subject to a force."

$$\vec{F}_{Laplace} = \sum \vec{f_i} = \sum q_i \vec{v_e} \times \vec{B} \tag{3}$$

$\sum \vec{f_i}$ corresponds to the sum of the Lorentz forces exerted on the moving electrons, $q$ the charge value of the electron ($q < 0$), $\vec{v}$ represents its velocity, and $\vec{B}$ represents the magnetic field generated by the primaries of the motor.

The force of Laplace is perpendicular to the plane containing $q\vec{v}$ and $\vec{B}$, its direction is determined by the rule of the right hand fingers, the thumb points in the direction of $q\vec{v}$ which corresponds to the direction of the induced current, the first finger points in the direction of the magnetic field, and the second finger points in the direction of the force (Fig. 9).

Ideally, the shape of the magnetic field in the air gap of the motor should be purely sinusoidal, because if the shape is composed of multiple harmonics, negative forces would be created on the plate in the opposite direction of the movement as illustrated in (Fig. 10). The more the harmonic content in the

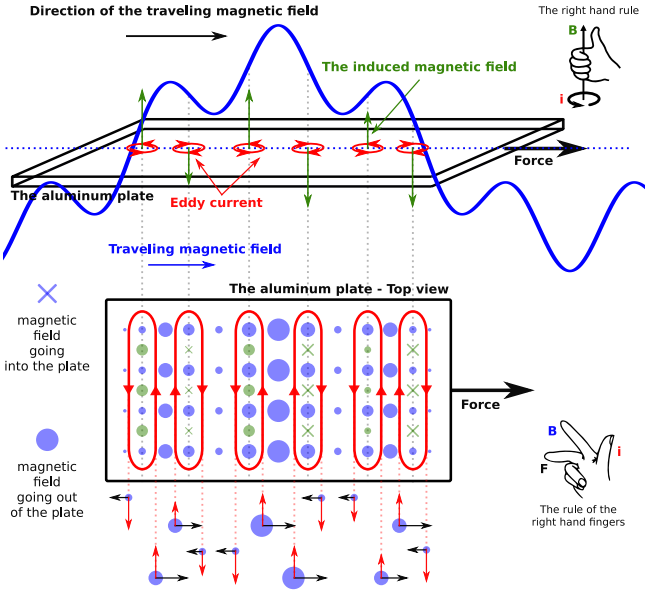


Figure 10: Non sinusoidal traveling magnetic field

traveling field, the greater the backward force is. And when the sheet secondary is thin, it tends to vibrate due to the presence of these harmonic components in the field.

# Chapter 5
# The Magnetic Field Distribution

## 5.1 Step-by-Step Analysis

In the step-by-step analysis, the flux at each tooth is calculated, taking into consideration the windings of the motor. Calculations using this method becomes laborious if the number of coils and phases is large.
Based on Lenz's Law:

$$\mathcal{E} = -\frac{\partial \Phi_B}{\partial t} \tag{4}$$

and relation between magnetic flux and magnetic field:

$$\Phi_B = BS \tag{5}$$

where $\mathcal{E}$ ,$\Phi_B$, $B$ and $S$ represent respectively the electromotive force ,the magnetic flux ,the magnetic field and surface.

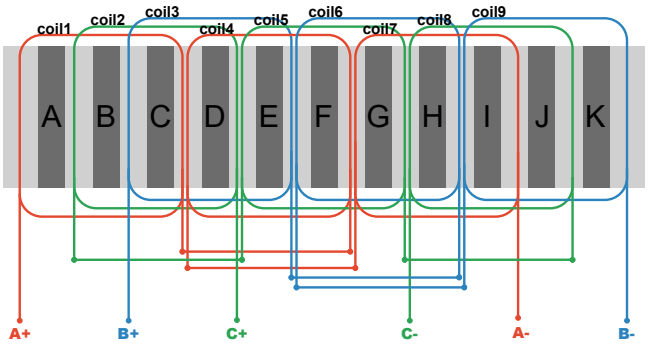


Figure 11: LIM Windings

Applying this principle on LIM having the coils in each phase connected in series, the following set of equations are obtained:

$$\begin{cases} \partial/\partial t(\Phi_A + \Phi_B + \Phi_C - \Phi_D - \Phi_E - \Phi_F + \Phi_G + \Phi_H + \Phi_I) = E_x \\ \partial/\partial t(-\Phi_B - \Phi_C - \Phi_D + \Phi_E + \Phi_F + \Phi_G - \Phi_H - \Phi_I + \Phi_J) = E_Y \\ \partial/\partial t(\Phi_C + \Phi_D + \Phi_E - \Phi_F - \Phi_G - \Phi_H + \Phi_I + \Phi_J + \Phi_K) = E_Z \end{cases} \tag{6}$$

Considering the double layer design of the LIM, and the series connection between the coils of each phase, The flux at each tooth is obtained, where $I_X$, $I_Y$, and $I_Z$ are the currents passing through the three phases of the motor.

$$
\begin{cases}
\Phi_A = {}^{4}\!/_{11} KI_X + {}^{3}\!/_{22} KI_Y - {}^{3}\!/_{22} KI_Z \\
\Phi_B = {}^{4}\!/_{11} KI_X - {}^{4}\!/_{11} KI_Y - {}^{3}\!/_{22} KI_Z \\
\Phi_C = {}^{4}\!/_{11} KI_X - {}^{4}\!/_{11} KI_Y + {}^{4}\!/_{11} KI_Z \\
\Phi_D = -{}^{7}\!/_{11} KI_X - {}^{4}\!/_{11} KI_Y + {}^{4}\!/_{11} KI_Z \\
\Phi_E = -{}^{4}\!/_{11} KI_X - {}^{7}\!/_{11} KI_Y + {}^{4}\!/_{11} KI_Z \\
\Phi_F = -{}^{7}\!/_{11} KI_X + {}^{7}\!/_{11} KI_Y - {}^{7}\!/_{11} KI_Z \\
\Phi_G = {}^{4}\!/_{11} KI_X + {}^{4}\!/_{11} KI_Y - {}^{7}\!/_{11} KI_Z \\
\Phi_H = {}^{4}\!/_{11} KI_X - {}^{4}\!/_{11} KI_Y - {}^{7}\!/_{11} KI_Z \\
\Phi_I = {}^{4}\!/_{11} KI_X - {}^{4}\!/_{11} KI_Y + {}^{4}\!/_{11} KI_Z \\
\Phi_J = -{}^{3}\!/_{22} KI_X - {}^{4}\!/_{11} KI_Y + {}^{4}\!/_{11} KI_Z \\
\Phi_J = -{}^{3}\!/_{22} KI_X + {}^{3}\!/_{22} KI_Y + {}^{4}\!/_{11} KI_Z
\end{cases} \tag{7}
$$

Based on 7 and 5, MATLAB simulation have been done.The figure below shows the result. It can be noticed the concentration of magnetic field is centered in the middle and that the magnetic field is not smoothly sinusoidal with respect to x direction.

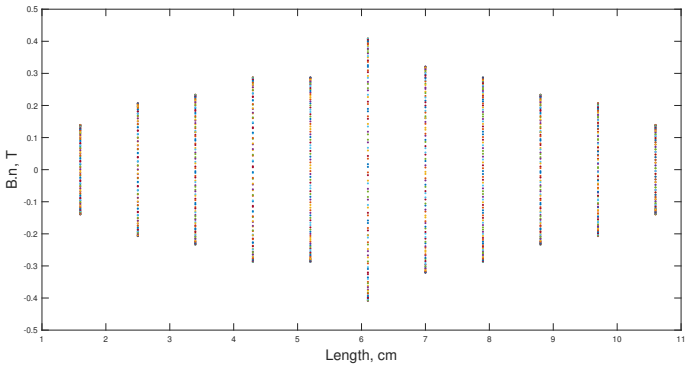


Figure 12: Shape of the magnetic field, using the step-by-step method calculation above each tooth

## 5.2 Finite Element Analysis

Finite Element Analysis (FEA) is a numerical method useful for solving problems with complicated geometries and materials properties. The accuracy with FEA is a lot higher than any analytical solution. Therefore FEA is necessary to understand the physical behavior of the motor, predict its performance, identify the weakness of the design, and determine the optimal design.
(the program used is FEMM)

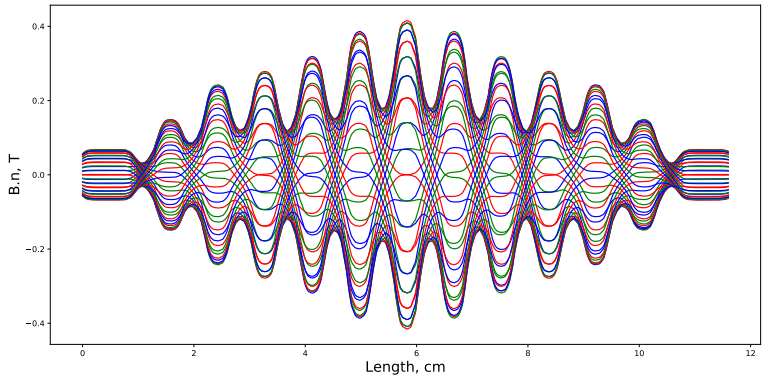


Figure 13: Shape of the magnetic field in the air gap of the motor along a period, using FEMM and Python

As in the step-by-step method, the profile of the distribution of the magnetic field is also unequally distributed, the magnetic field is dominant in the center and decreases more and more towards the extremities. The simulation with FEA gives not only the magnetic in each tooth but also the shape of the magnetic field all along the length of the air gap, including the slots. Thus a better representation of the magnetic field is formed. It can be seen from (Fig. 13) that the magnetic field is not uniformly distributed along a period over the length of the stator. Therefore it can be inferred that the shape of the traveling magnetic field is not sinusoidal and but rather composed of harmonic components.

## 5.3 The Winding design and the offset between the two primaries of the motor

The winding design of any motor has an important effect on its efficiency and behavior. The shape of the magnetic fields is directly related to the winding design and also to the input signal. There are mainly two types of windings design: the planar non-overlapping windings and the double layer windings.

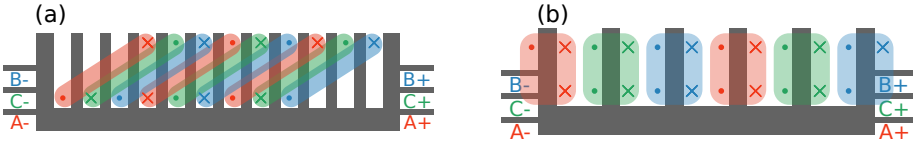


Figure 14: (a) Three phased double layer winding LIM, (b) Three phased tabular winding LIM

Linear induction motors with double layer stator windings provide a good traveling magnetic field with little harmonic content. One disadvantage of this type of windings is that half fitted slots around the ends of the stators are found. Planar windings on the other hand, are very cost effective and all the slots have windings equitably distributed. However, they deliver a lousier traveling magnetic field with a lot of harmonic content.

The harmonic content thus are due to the motor winding design. In particular, the magnetic field is composed of two large sinusoidal field, the fundamental and the second harmonic. The second harmonic of the field travels in the opposite direction of that of the generated field and its fundamental. And this backward traveling field is the one responsible for the generation of the negative force.

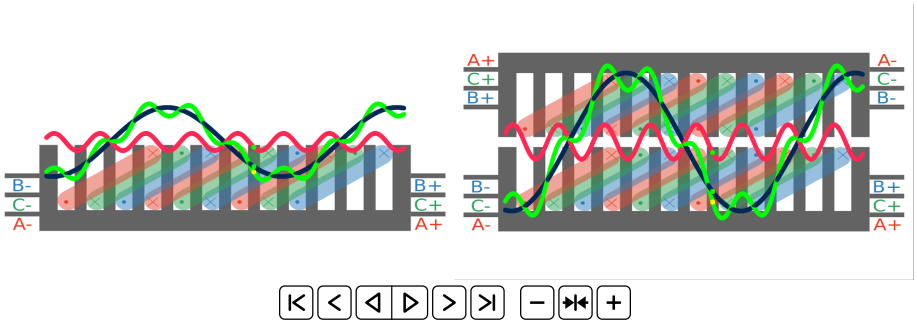


Figure 15: The fundamental (dark blue) and the second harmonic (magenta) of the traveling magnetic field (Green). SLIM Vs. DSLIM.

With a much more complicated winding design and multi-phased motor, the shape of the traveling magnetic field would be enhanced but not to a purely sinusoidal form.

Having two symmetric SLIMs in a DSLIM each generating its own traveling magnetic field that can be thought as a combination two signals. Thus, by offsetting the position of one side of the motor with respect to the other by $\tau/u$, where $u$ is the ratio of the second harmonic to the fundamental, we can eliminate the second undesired harmonic that is causing the plate to vibrate.

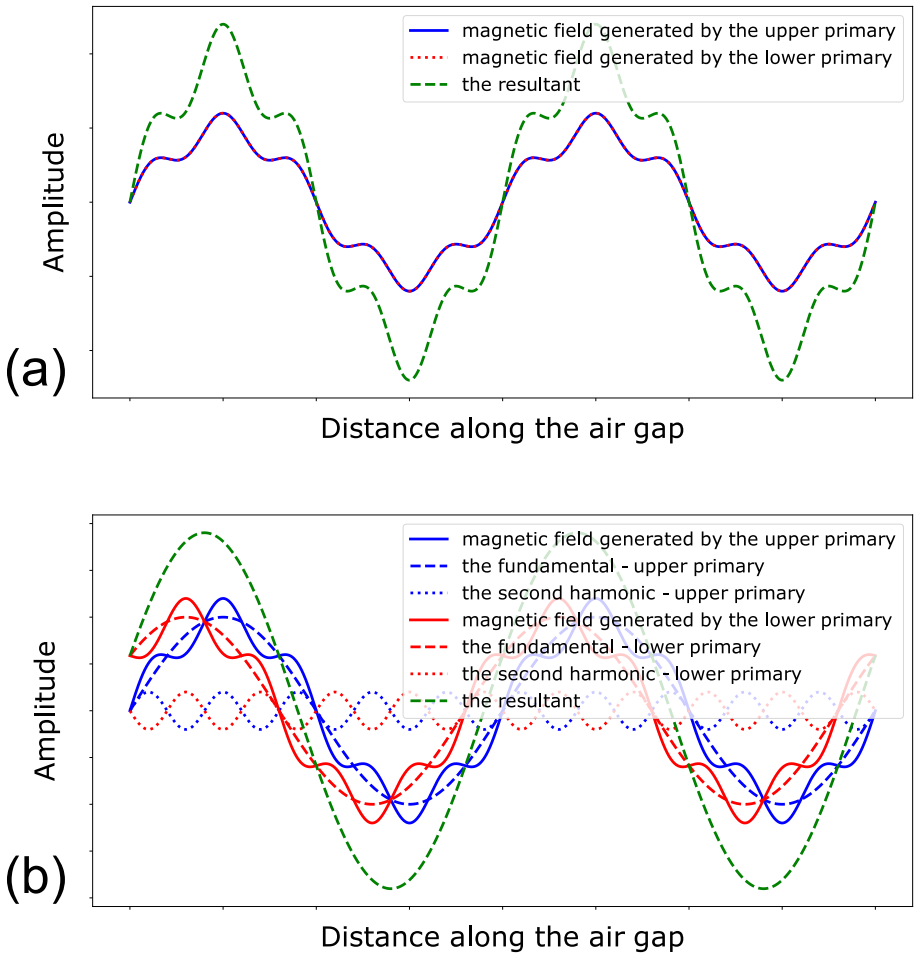


Figure 16: (a) primaries not shifted, (b) primaries shifted

It can be seen in (Fig. ) that the resultant has a sine wave shape. After eliminating the second harmonic we will end up with two sine waves of the same frequency (the fundamental frequency) and with a phase shift between them of $\pi/u$ and we know that the sine wave shape will be retained if two sine waves of the same frequency and arbitrary phase were added.

### 5.3.1 FEM Simulation, no shift between primaries

FEM simulation of a Double Sided Linear Induction Motor that shows the shape of the magnetic field in the air gap of the motor.

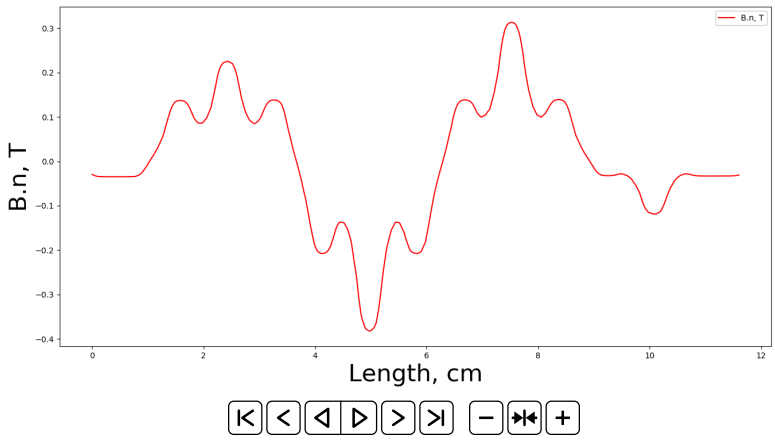


Figure 17: Shape of the magnetic field between the two primaries of the motor

### 5.3.2 FEM Simulation, with a shift between primaries

FEM simulation showing the shape of the traveling magnetic field in the air gap of a DSLIM with an offset between its two primaries.

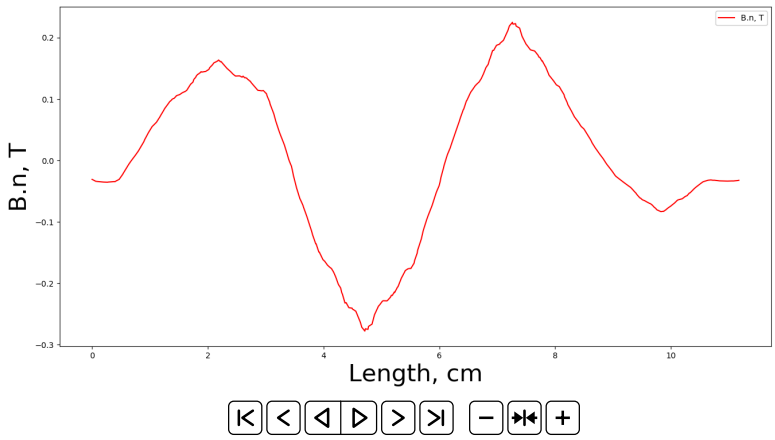


Figure 18: Shape of the magnetic field between the two primaries of a shifted DSLIM

## 5.4 How harmonics generate force vibration ?

The generated force is a result of Laplace law presented by this equation:

$$Fav = \int_0^{2a} \int_{x_1}^{x_2} Re(j^* \mu_0 H_y(x,t))\ dx\ dz \tag{8}$$

Due to the presence of second harmonic in magnetic field an eddy current is generated with harmonics based on Maxwell Equation 39.

$$Fav = \int_0^{2a} \int_{x_1}^{x_2} \mu_0 Re((j_1^* + j_2^* + .... + j_n^*)(H_{y1} + H_{y2} + .... + H_{yn})(x,t))\ dx\ dz \tag{9}$$

That lead to a multiplication of eddy current and magnetic field with different order.
In this example,the secondary will have a tilt equal to zero .

$$Fav = 2a \int_0^{\tau} \mu_0 Re((j_1^* + j_2^*)(H_{y1} + H_{y2})(x,t))\ dx \tag{10}$$

$$Fav = F_1 + F_2 + F_3 + F_4 \tag{11}$$

where,

$$
\begin{aligned}
F_1 &= 2a \int_0^{\tau} \mu_0 Re(j_1^* H_{y1}(x,t))\ dx \\
F_2 &= 2a \int_0^{\tau} \mu_0 Re(j_2^* H_{y2}(x,t))\ dx \\
F_3 &= 2a \int_0^{\tau} \mu_0 Re(j_1^* H_{y2}(x,t))\ dx \\
F_4 &= 2a \int_0^{\tau} \mu_0 Re(j_2^* H_{y1}(x,t))\ dx
\end{aligned}
\tag{12}
$$

Based on FEM ,the second harmonic has a period equal to 5.2 of the first harmonic.Eddy current is the mirror of the magnetic field and It will have the same harmonics order but with different amplitude and a phase.As a result the Fav component 12 will be:

$$
\begin{aligned}
F_1 &= Re(2a \int_0^{2\tau} A \exp(-j(2\pi ft - \frac{\pi}{\tau}x)) B \exp j(2\pi ft - \frac{\pi}{\tau}x + \varphi)\ dx) \\
F_2 &= Re(2a \int_0^{2\tau} \frac{A}{3} \exp(-5.2j(2\pi ft - \frac{\pi}{\tau}x)) \frac{B}{3} \exp(5.2j(2\pi ft - \frac{\pi}{\tau}x + \varphi^{'}))\ dx) \\
F_3 &= Re(2a \int_0^{2\tau} A \exp(-j(2\pi ft - \frac{\pi}{\tau}x)) \frac{B}{3} \exp(5.2j(2\pi ft - \frac{\pi}{\tau}x + \varphi^{'}))\ dx) \\
F_4 &= Re(2a \int_0^{2\tau} \frac{A}{3} \exp(-5.2j(2\pi ft - \frac{\pi}{\tau}x)) B \exp j(2\pi ft - \frac{\pi}{\tau}x + \varphi)\ dx)
\end{aligned}
\tag{13}
$$

As a result we will get:

$$
\begin{aligned}
F_1 &= 4a\tau AB \\
F_2 &= 4a\tau \frac{AB}{9} \cos\varphi^{'} \\
F_3 &= \frac{8a\tau}{4.2\pi} \frac{AB}{3} \sin(0.2\pi) \cos(4.2(2\pi ft - \frac{\pi}{\tau}x) + 5.2\varphi^{'} - 0.1\pi) \\
F_4 &= \frac{8a\tau}{4.2\pi} \frac{AB}{3} \sin(0.2\pi) \cos(4.2(2\pi ft - \frac{\pi}{\tau}x) - \varphi - 0.1\pi)
\end{aligned}
\tag{14}
$$

The generated force is composed of $F_1$ accompanied with negative force $F_2$ and 2 oscillating force with respect to time $F_3$,$F_4$. As a result of this phenomena a vibration and a decrease in force occur.
N.B:The magnetic field is mainly composed of two sinusoidal waves the fundamentals and the second.We might have in addition other harmonics with a lower amplitude and high frequency which we consider negligible in our case.In other winding designs these harmonics may have an effect.

## 5.5 The length of the motor and the number of poles

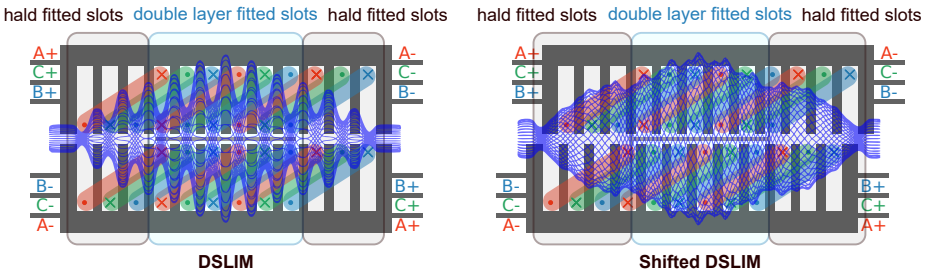


Figure 19: DSLIM Vs shifted DSLIM. Magnetic field distribution over a period along the air gap of the motor.

The number of poles, the pole pitch, the length of the secondary, and the length of the primaries have a significant influence on the efficiency of the system. The proper choice of these four parameters significantly reduces the end effect and increase efficiency.

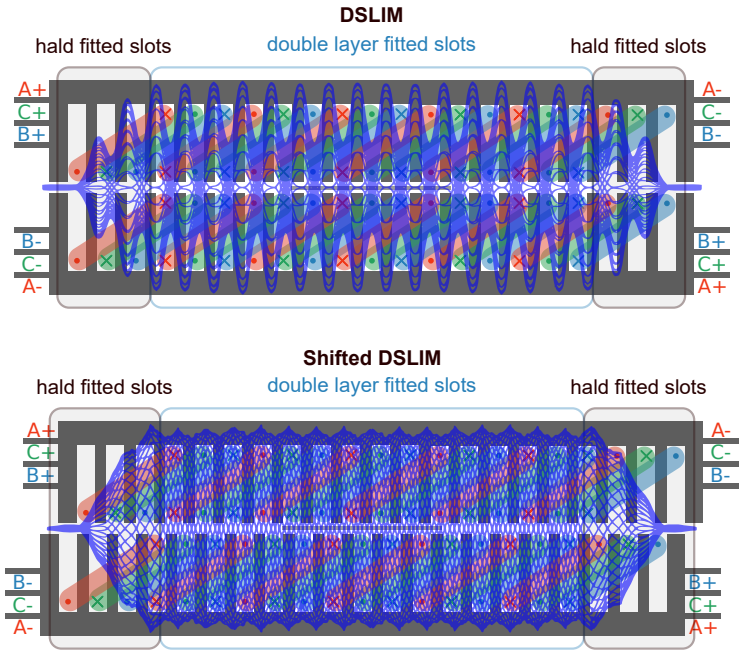


Figure 20: Longer DSLIM Vs Longer Shifted DSLIM. Magnetic field distribution over a period along the air gap of the motor.

### 5.5.1 FEM Simulation, of a 6 poles pitches long DSLIM with a shift between primaries

FEM simulation showing the shape of the traveling magnetic field in the air gap of a DSLIM with an offset between its two primaries.

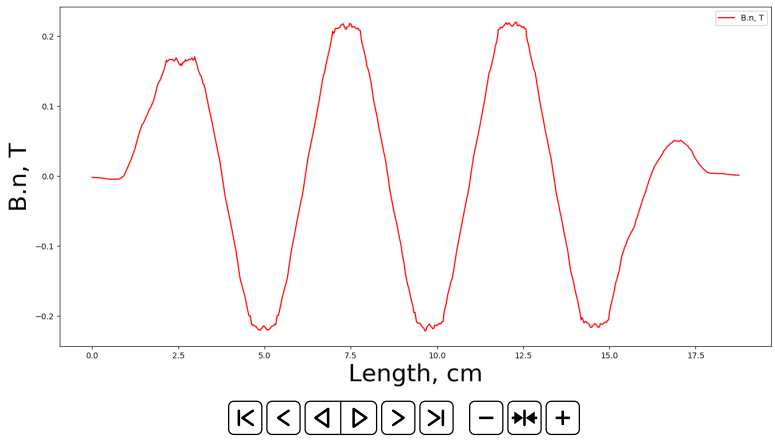


Figure 21: Shape of the magnetic field between the two primaries of a shifted DSLIM

FEM simulation showing the shape of the traveling magnetic field in the air gap of a DSLIM with an offset between its two primaries.

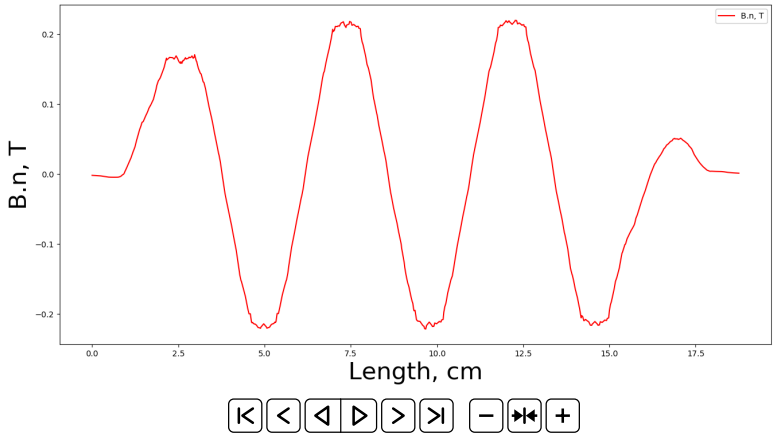


Figure 22: Shape of the magnetic field between the two primaries of a shifted DSLIM

# Chapter 6
# DSLIM equations

## 6.1 The slip of the motor

The Slip of the motor is the difference between the speed of the traveling magnetic field generated by the primaries of the motor and the speed of the secondary. The slip is given by:

$$s = \frac{V_s - V_r}{V_s} \tag{15}$$

$V_r$ is the velocity of the secondary and $V_s$ is the synchronous velocity of the motor given by:

$$V_s = 2f\tau \tag{16}$$

Where, $\tau$ is the pole pitch of the motor, the distance between two neighboring poles as seen in figure. $\tau$ is equal to the length of the linear motor $M_L$ divided by the number of poles $p$

$$\tau = \frac{M_L}{p} \tag{17}$$

## 6.2 Depth penetration

Eddy currents induced in the secondary by the traveling magnetic field generated by the primaries concentrate on the surface of the secondary and decrease in strength exponentially with depth. The depth that eddy currents penetrate is affected by the frequency and intensity of the traveling field, and the conductivity and magnetic permeability of the conductor. The extent of penetration decreases with an increase in frequency, conductivity, and magnetic permeability.

The depth at which eddy current density has decreased to $1/e$, or about 37% of the surface density, is called the standard depth of penetration $\delta$.

$$\delta \approx \frac{1}{\sqrt{\pi f \mu \sigma}} \tag{18}$$

$K_j$ is the correction coefficient, considering the secondary skin effect. Given by the following expression:

$$K_j = \frac{d}{2\delta}\left[\frac{\mathrm{sh}\left(\frac{d}{\delta}\right) + \sin\left(\frac{d}{\delta}\right)}{\mathrm{ch}\left(\frac{d}{\delta}\right) - \cos\left(\frac{d}{\delta}\right)}\right] \tag{19}$$

where $d$ is the thickness of the secondary, and $\delta$ is the field depth penetration.The effective conductivity $\sigma_2$ is thus expressed as:

$$\sigma_2 = \sigma / K_j \tag{20}$$

## 6.3 The effective air gap

The air gap is an important parameter in Linear Induction Motor Design. $g$ is the physical air gap, the distance that separates the two primaries. The air gap g is corrected by carter's coefficient $K_c$ considering the slotted structure of the primary. The length of the air gap considering the slotting $g'$ is obtained by:

$$g' = K_c g \tag{21}$$

Where

$$K_c = \frac{\lambda}{\lambda - \gamma g} \tag{22}$$

Where $\lambda$ is the distance between the centers of two consecutive teeth, and $\gamma$ which has as expression: (ref)

$$\gamma = \frac{4}{\pi}\left[\frac{w_s}{2g}\arctan\left(\frac{w_s}{2g}\right) - \ln\sqrt{1+\left(\frac{w_s}{2g}\right)^2}\right] \tag{23}$$

The effective air gap length $g_e$ is equal to the product of $g'$ and $k_g$, the correction factor accounting for uninformed of y-component of the field along y-direction in cases when x-component of the field could not be ignored. (ref)

$$g_e = K_g g' \tag{24}$$

With

$$k_g = \frac{\operatorname{sh}\dfrac{\pi g'}{\tau}}{\dfrac{\pi g'}{\tau}} \tag{25}$$

## 6.4 The winding factor

The winding factor, $K_w$, is the product of the pitch factor, $K_p$, and the distribution factor, $K_d$.

$$k_w = k_p k_d \tag{26}$$

The pitch factor $K_p$ is given by:

$$k_p = \sin\left(\frac{\theta_p}{2}\right) \tag{27}$$

$\theta_p$ is the coil span in electric degrees. if the coil span is equal to the pole pitch of the motor which corresponds to 180 degree electrical, $K_p$ becomes equal to one.

The distribution factor $K_d$ is given by:

$$k_d = \frac{\sin(\frac{q_1\alpha}{2})}{q_1 \sin(\frac{\alpha}{2})} \tag{28}$$

$\alpha$ is the slot angle in electrical degrees given as:

$$\alpha = \frac{\pi}{mq_1} \tag{29}$$

$q_1$ is the number of slots-per-pole-per-phase in the stator iron core.

$$k_w = k_p k_d = \frac{\sin(\frac{q_1\alpha}{2})}{q_1 \sin(\frac{\alpha}{2})} \sin\left(\frac{\theta_p}{2}\right) \tag{30}$$

If $k_d$ is equal to one, we obtain:

$$k_w = \frac{\sin\left(\frac{\pi}{2m}\right)}{q_1 \sin\left(\frac{\pi}{2mq_1}\right)} \tag{31}$$

## 6.5 The Goodness factor

The performance of a Linear Induction Motor is affected by many parameters. These parameters should be taken into consideration in the design of the motor. The goodness factor is a metric used to determine the performance of LIMs.

$$G = \frac{\mu_0 \sigma_s \omega \tau^2}{g_e \pi^2} \tag{32}$$

$G$ is a powerful variable in the design by reason of considering geometrical and physical variables .

## 6.6 The current sheet in the air gap

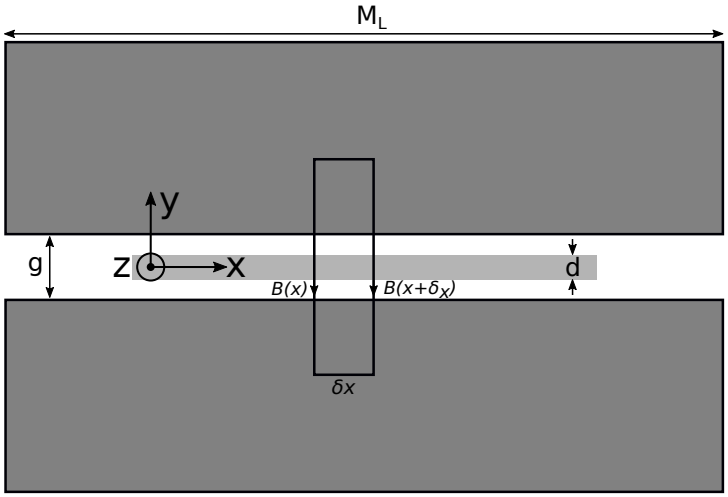


Figure 23: Elementary loop in the xy plane

Electromagnetic equations of the motor taking relative motion between the primary and the secondary are summarized as follows:

$$\nabla \times \mathbf{H} = \mathbf{J}_s + \mathbf{J}_r \quad with \quad \mathbf{J}_r = \sigma(\mathbf{E} + \mathbf{v} \times \mathbf{B}) \tag{33}$$

where $\mathbf{H}$ is the magnetic field intensity, $\mathbf{B}$ is the magnetic flux density, $\mathbf{E}$ is the electric field intensity, $\mathbf{J}_\mathrm{s}$ and $\mathbf{J_r}$ are the volume current density of the primary and the secondary, respectively, $\mathbf{v}$ is the relative velocity between the primary and the secondary. In 1-D analysis we obtain the following equation in with all vectors are only in function of x and time t.

$$g_e \frac{\partial H_y}{\partial x} = j_{s1} + j_{r1} \tag{34}$$

## 6.7 The surface current density of the primary

The current carried out by the windings of the motor can be replaced by a thin fictitious layer of current, called the "current sheet", distributed over the surface of the stator facing the air gap. The complex form of surface current density for the primary can be expressed as:

$$j_{s1} = J_{sm} \exp j \left( \omega t - \frac{\pi}{\tau} x \right) \tag{35}$$

Its amplitude $J_{sm}$ is

$$J_{sm} = \frac{m_1 \left(2 w_1 k_{w1}\right) \sqrt{2} I_1}{M_L} \tag{36}$$

The current sheet strength, $J_{sm}$, is therefore the amount of current per stator length (amp/meter). $m$ is the number of phases, $k_{w1}$ is the winding factor, $w_1$ is the number of series turns per phase, $I_1$ is the RMS value of the input current, and $L_s$ is the length of the stator.

## 6.8 The surface current density of the secondary

The surface current density for the secondary $j_{r1}$ is given by:

$$j_{r1} = \sigma_s \left( E_z + v_x B_y \right) \tag{37}$$

where $\sigma_s = \sigma_2 d$ d is the effective surface conductivity for the secondary, $v_x$ is the speed of the secondary.
From the Maxwell–Faraday equation which states that magnetic field variation with respect to time always accompanies a non-conservative electric field, and vice versa.

$$\nabla \times \mathbf{E} = -\frac{\partial \mathbf{B}}{\partial t} \tag{38}$$

In x-direction ,we obtain:

$$\frac{\partial E_z}{\partial x} = \frac{\partial B_y}{\partial t} = \mu_0 \frac{\partial H_y}{\partial t} \tag{39}$$

Substituting 35 36 37 39 leads to a second order differential equation representing the magnetic flux in the air-gap:

$$\frac{\partial^2 H_y}{\partial x^2} - \mu_0 \sigma_e v_x \frac{\partial H_y}{\partial x} - \mu_0 \sigma_e \frac{\partial H_y}{\partial t} = -j \frac{\pi}{\tau} \frac{J_{sm}}{g_e} \exp j \left( \omega t - \frac{\pi}{\tau} x \right) \tag{40}$$

where $\sigma_e = \dfrac{\sigma_s}{g_e} = \dfrac{\sigma_2 d}{g_e}$

The general field solution in the air gap is:

$$\begin{aligned} H_y(x,t) =& H_{ym} \exp j \left( \omega t - \frac{\pi}{\tau} x + \varphi \right) \\ &+ C_1 \exp \left( -\frac{x}{\lambda_1} \right) \exp j \left( \omega t - \frac{\pi}{\tau_e} x \right) \\ &+ C_2 \exp \left( \frac{x}{\lambda_2} \right) \exp j \left( \omega t + \frac{\pi}{\tau_e} x \right) \end{aligned} \tag{41}$$

The field intensity in the air gap is composed into three parts.The first term is the normal traveling wave, which moves at synchronous speed. The second and the last term is the entry-end forward and the exit-end backward traveling wave, which attenuates along x-direction and whose attenuation constant is $\lambda_1$ and $\lambda_2$,respectively.
where:

$$H_{ym} = \frac{J_{sm} \tau}{g_e \pi \sqrt{1 + (SG)^2}} \tag{42}$$

$$\varphi = \tan^{-1}\left(\frac{1}{sG}\right) \tag{43}$$

in which, $C_1$ and $C_2$ are integral constants determined from the boundary conditions.

the factors in (13) are defined as follows:

$$\lambda_1 = \frac{2}{\mu_0 \sigma_e v_x \left(\alpha_1 - 1\right)} \tag{44}$$

$$\lambda_2 = \frac{2}{\mu_0 \sigma_e v_x \left(\alpha_1 + 1\right)} \tag{45}$$

$$\tau_e = \frac{2\pi}{\mu_0 \sigma_e v_x \alpha_2} \tag{46}$$

where

$$\alpha_1 = \sqrt{\frac{1}{2}\left[1 + \sqrt{\left(\frac{4\omega}{\mu_0 \sigma_e v_x^2}\right)^2 + 1}\right]} \tag{47}$$

$$\alpha_2 = \sqrt{\frac{1}{2}\left[-1 + \sqrt{\left(\frac{4\omega}{\mu_0 \sigma_e v_x^2}\right)^2 + 1}\right]} \tag{48}$$

Due to discontinuity in the secondary,the last two end effect exist(Entry and exit effect)in LIM(In Rotary Machine doesn't exist).Their superimposition upon the normal wave deform the flux distribution and consequently the performance of the motor. To evaluate the integral constants $C_1$ and $C_2$ , we divide the analysis model into three regions, which is shown in Fig. The tangential components of the magnetic field intensity are considered to be continuous at two edges, $x = 0$ and $x = 2p\tau$, that is:

$$\begin{array}{l} H_{y1}\Big|_{x=0} = H_{y2}\Big|_{x=0} \\ H_{y1}\Big|_{x=2p\tau} = H_{y3}\Big|_{x=2p\tau} \end{array} \tag{49}$$

where the subscript numbers identify the regions. Using the above boundary conditions, $C_1$ and $C_2$ can be determined as follows:

$$C_1 = \frac{jJ_{sm}\tau}{g_e \pi \Delta}\left[\frac{jsG\left(1 - \exp\left(Q_2\right)\right)}{1 + jsG}\right] \tag{50}$$

$$C_2 = \frac{jJ_{sm}\tau}{g_e \pi \Delta}\left[\frac{jsG\left(\exp\left(-Q_1\right) - 1\right)}{1 + jsG}\right] \tag{51}$$

where

$$\Delta = \exp\left(-Q_1\right) - \exp\left(Q_2\right) \tag{52}$$

$$Q_1 = \left(\frac{1}{\lambda_1} + j\frac{\pi}{\tau_e}\right) 2p\tau \tag{53}$$

$$Q_2 = \left(\frac{1}{\lambda_2} + j\frac{\pi}{\tau_e}\right) 2p\tau \tag{54}$$

## Chapter 7
## Force with respect to angel

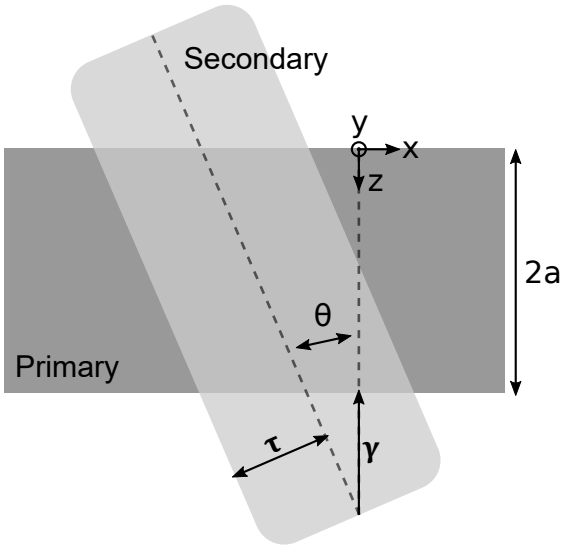


Figure 24: Tilted secondary with respect to primary

Applying Laplace principle on the common surface between the primary and the secondary we get average thrust force(in Newton):

$$Fav = \int_0^{2a} \int_{x_1}^{x_2} Re(j^* \mu_0 H_y(x,t))\ dx\ dz \tag{55}$$

We have calculated the force when $\theta$ is positive, we get by symmetry the same force when $\theta$ is negative.

$$x_2 = \tan(\theta) z + b_2 \tag{56}$$

for

$$z = 2a, \quad x_2 = -\gamma \tan(\theta) + \frac{\tau}{\cos\theta} + \tau \tag{57}$$

$$b_2 = -\gamma \tan(\theta) + \tau(\frac{1}{\cos\theta} + 1) - \tan(\theta) 2a \tag{58}$$

$$x_1 = \tan(\theta) z_1 + b_1 \tag{59}$$

for

$$z = 2a, \qquad x_1 = -\gamma \tan(\theta) - \frac{\tau}{\cos\theta} + \tau \tag{60}$$

$$b_1 = \tau(1 - \frac{1}{\cos\theta}) - \gamma \tan(\theta) - \tan(\theta)2a \tag{61}$$

$$\begin{aligned} Fav = \int_0^{2a} \int_{x_1}^{x_2} Re(J_{sm}\mu_0(H_{ym} \exp j\,(\varphi) \\ + C_1 \exp\left(-\frac{x}{\lambda_1}\right) \exp j\left((\frac{\pi}{\tau} - \frac{\pi}{\tau_e})x\right) \\ + C_2 \exp\left(\frac{x}{\lambda_2}\right) \exp j\left((\frac{\pi}{\tau} + \frac{\pi}{\tau_e})x\right))\ dx\ dz \end{aligned} \tag{62}$$

$$\begin{aligned} Fav = \int_0^{2a} Re(J_{sm}\mu_0(H_{ym} \exp j\,(\varphi)\,(b_2 - b_1) \\ + \frac{C_1}{\frac{-1}{\lambda_1} + (\frac{\pi}{\tau} - \frac{\pi}{\tau_e})x} \exp\left(-\frac{x}{\lambda_1}\right) \exp j\left((\frac{\pi}{\tau} - \frac{\pi}{\tau_e})x\right)\Big|_{x_1}^{x_2} \\ + \frac{C_2}{\frac{1}{\lambda_2} + (\frac{\pi}{\tau} + \frac{\pi}{\tau_e})x} \exp\left(\frac{x}{\lambda_2}\right) \exp j\left((\frac{\pi}{\tau} + \frac{\pi}{\tau_e})x\right)\Big|_{x_1}^{x_2}))\ dz \end{aligned} \tag{63}$$

$$Fav = \int_0^{2a} Re(J_{sm}\mu_0(\beta + \frac{C_1}{\frac{-1}{\lambda_1} + (\frac{\pi}{\tau} - \frac{\pi}{\tau_e})}T + \frac{C_2}{\frac{1}{\lambda_2} + (\frac{\pi}{\tau} + \frac{\pi}{\tau_e})}W))\ dz \tag{64}$$

where

$$\beta = H_{ym} \exp j\,(\varphi)\,(b_2 - b_1) \tag{65}$$

$$T = \exp\left(-\frac{x}{\lambda_1}\right) \exp j\left((\frac{\pi}{\tau} - \frac{\pi}{\tau_e})x\right)\Big|_{x_1}^{x_2} \tag{66}$$

$$W = \exp\left(\frac{x}{\lambda_2}\right) \exp j\left((\frac{\pi}{\tau} + \frac{\pi}{\tau_e})x\right)\Big|_{x_1}^{x_2} \tag{67}$$

Integrating 65 66 67 We will get :

$$\int_0^{2a} \beta\ dz = \frac{4a\tau}{cos(\theta)} H_{ym} \exp j(\varphi) \tag{68}$$

$$\begin{aligned} \int_0^{2a} T\ dz = &\frac{1}{tan(\theta)(\frac{-1}{\lambda_1} + j(\frac{\pi}{\tau} - \frac{\pi}{\tau_e}))}\Big(\exp\Big((2a)tan(\theta)(\frac{-1}{\lambda_1} + j(\frac{\pi}{\tau} - \frac{\pi}{\tau_e}))\Big) - 1\Big) \\ &\left[\exp(b_2(\frac{-1}{\lambda_1} + j(\frac{\pi}{\tau} - \frac{\pi}{\tau_e}))) - \exp(b_1(\frac{-1}{\lambda_1} + j(\frac{\pi}{\tau} - \frac{\pi}{\tau_e})))\right] \end{aligned} \tag{69}$$

$$\int_0^{2a} W\ dz = \frac{1}{tan(\theta)(\frac{1}{\lambda_2} + j(\frac{\pi}{\tau} + \frac{\pi}{\tau_e}))} \Big( \exp\Big((2a)tan(\theta)(\frac{1}{\lambda_2} + j(\frac{\pi}{\tau} - \frac{\pi}{\tau_e}))\Big) - 1\Big) \left[ \exp(b_2(\frac{1}{\lambda_2} + j(\frac{\pi}{\tau} + \frac{\pi}{\tau_e}))) - \exp(b_1(\frac{1}{\lambda_2} + j(\frac{\pi}{\tau} + \frac{\pi}{\tau_e}))) \right] \tag{70}$$

In electrical machine mechanical force and magneto motive force are equal. Only the losses will be with respect to the velocity of the secondary. NB:We don't care about velocity since in haptic interface velocity is very low.

# Chapter 8
# Equivalent circuit with $\theta$

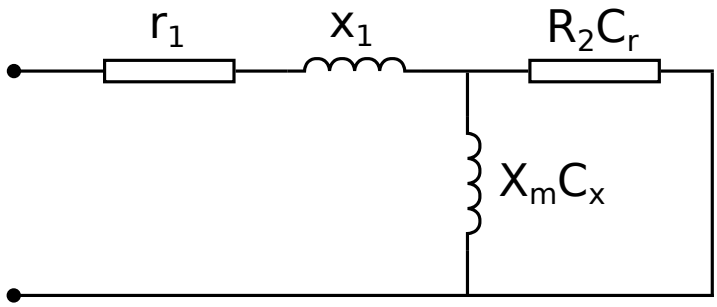


Figure 25: DSLIM equivalent circuit

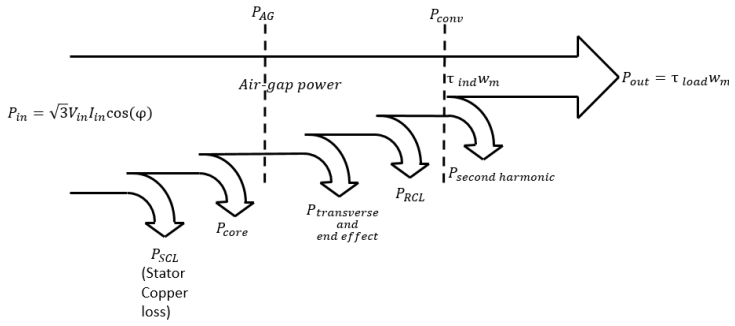


Figure 26: The power-flow of an induction motor

## 8.1 Losses and the Power-Flow Diagram

The input power $P_{in}$ is in the from of three-phase electric voltages and currents.The first two losses are the primary copper loss(Ppcl) and hysteresis and eddy currents in the primary.The remaining power at this point is transferred to the rotor.This power is called the air gap power $P_{AG}$.After this power is transferred to the secondary,some of it is lost as transverse effect,end effect and secondary copper losses,and the rest is converted from electrical to mechanical power($P_{conv}$).Finally,second harmonic signal generates an opposite force.The remaining power is the output of the motor $P_{out}$.

## 8.2 RIM vs LIM

In rotary induction motors , $R_{Fe}$ represents the core losses which is negligible in linear motor because a realistic air-gap flux density leads to moderate flux densities in the core and hence,rather low core losses. Therefore,it will not be taken into consideration in the equivalent circuit of LIM.
The second difference is the slip range.Due to haptic interface application,the secondary velocity is low and the slip is nearly one.So the generated heat in the secondary effects the velocity of the secondary but mechanical force will remain equal to electromotive force.As a result,we don't need to split the secondary resistance into mechanical power and secondary copper losses.
A third difference is the absence of mechanical losses.An air bearing is implemented in order to reduce the friction.

## 8.3 LIM Parameters

Complex electromotive force power is the summation of laplacian force multiplied primary velocity on each point of the common surface.

$$\begin{aligned}
S_{emf} =& v_s \int_0^{2a} \int_{x_1}^{x_2} Re(j^* \mu_0 H_y(x,t))\ dx\ dz \\
&= v_s \mu_0 Jsm \Bigg[ \frac{4a\tau}{cos(\theta)} H_{ym} \exp j(\varphi) \\
&+ \frac{C_1}{\frac{-1}{\lambda_1} + (\frac{\pi}{\tau} - \frac{\pi}{\tau_e})} \frac{1}{tan(\theta)(\frac{-1}{\lambda_1} + j(\frac{\pi}{\tau} - \frac{\pi}{\tau_e}))} \Big( \exp\Big((2a) tan(\theta)(\frac{-1}{\lambda_1} + j(\frac{\pi}{\tau} - \frac{\pi}{\tau_e}))\Big) - 1 \Big) \\
&\Bigg[ \exp(b_2(\frac{-1}{\lambda_1} + j(\frac{\pi}{\tau} - \frac{\pi}{\tau_e}))) - \exp(b_1(\frac{-1}{\lambda_1} + j(\frac{\pi}{\tau} - \frac{\pi}{\tau_e}))) \Bigg] \\
&+ \frac{C_2}{\frac{1}{\lambda_2} + (\frac{\pi}{\tau} + \frac{\pi}{\tau_e})} \frac{1}{tan(\theta)(\frac{1}{\lambda_2} + j(\frac{\pi}{\tau} + \frac{\pi}{\tau_e}))} \Big( \exp\Big((2a) tan(\theta)(\frac{1}{\lambda_2} + j(\frac{\pi}{\tau} - \frac{\pi}{\tau_e}))\Big) - 1 \Big) \\
&\Bigg[ \exp(b_2(\frac{1}{\lambda_2} + j(\frac{\pi}{\tau} + \frac{\pi}{\tau_e}))) - \exp(b_1(\frac{1}{\lambda_2} + j(\frac{\pi}{\tau} + \frac{\pi}{\tau_e}))) \Bigg] \Bigg]
\end{aligned} \tag{71}$$

Taking $J_{sm}$ Outside of $H_{ym}$ , $C_1$ and $C_2$ W get

$$H_{ym} = H_{ym}^{'} J_{sm} \tag{72}$$

$$C_1 = C_1^{'} J_{sm} \tag{73}$$

$$C_2 = C_2^{'} J_{sm} \tag{74}$$

equation 75 will take a new form

$$
\begin{aligned}
S_{emf} =& v_s \mu_0 J s m^2 \Bigg[ \frac{4a\tau}{cos(\theta)} H_{ym}^{'} \exp j(\varphi) \\
&+ \frac{C_1^{'}}{\frac{-1}{\lambda_1} + (\frac{\pi}{\tau} - \frac{\pi}{\tau_e})} \frac{1}{tan(\theta)(\frac{-1}{\lambda_1} + j(\frac{\pi}{\tau} - \frac{\pi}{\tau_e}))} \Big( \exp\Big((2a) tan(\theta)(\frac{-1}{\lambda_1} + j(\frac{\pi}{\tau} - \frac{\pi}{\tau_e}))\Big) - 1\Big) \\
&\Bigg[ \exp(b_2(\frac{-1}{\lambda_1} + j(\frac{\pi}{\tau} - \frac{\pi}{\tau_e}))) - \exp(b_1(\frac{-1}{\lambda_1} + j(\frac{\pi}{\tau} - \frac{\pi}{\tau_e}))) \Bigg] \\
&+ \frac{C_2^{'}}{\frac{1}{\lambda_2} + (\frac{\pi}{\tau} + \frac{\pi}{\tau_e})} \frac{1}{tan(\theta)(\frac{1}{\lambda_2} + j(\frac{\pi}{\tau} + \frac{\pi}{\tau_e}))} \Big( \exp\Big((2a) tan(\theta)(\frac{1}{\lambda_2} + j(\frac{\pi}{\tau} - \frac{\pi}{\tau_e}))\Big) - 1\Big) \\
&\Bigg[ \exp(b_2(\frac{1}{\lambda_2} + j(\frac{\pi}{\tau} + \frac{\pi}{\tau_e}))) - \exp(b_1(\frac{1}{\lambda_2} + j(\frac{\pi}{\tau} + \frac{\pi}{\tau_e}))) \Bigg] \Bigg]
\end{aligned} \tag{75}
$$

$$S_{emf} = J_{sm}^2 (P_i^{'} + Q_i^{'}) \tag{76}$$

$$P_i^{'} = Re(\frac{S_{emf}}{J_{sm}^2}) \tag{77}$$

$$Q_i^{'} = Im(\frac{S_{emf}}{J_{sm}^2}) \tag{78}$$

Based on equation 76 and electrical machine equivalent circuit principle.

$$R_2 = \frac{2 * m_1 (w_1 K_{w1})^2 (P_i^{'^2} + Q_i^{'^2})}{P_i^{'} (p\tau)^2} \tag{79}$$

$$X_m = \frac{2 * m_1 (w_1 K_{w1})^2 (P_i^{'^2} + Q_i^{'^2})}{Q_i^{'} (p\tau)^2} \tag{80}$$

$r_1$ and $X_1$ represent the impedance of a single phase.

$$r_1 = \rho_w l_w / A_{wt} \tag{81}$$

where,$\rho_w$ is the volume resistivity of the copper wire in the sator winding,$l_w$ length of the copper wire per phaseand $A_{wt}$ is the cross-sectional area of the wire.

$$l_w = N_1 l_{w1} \tag{82}$$

$$l_{w1} + 2(W_s + l_{ce}) \tag{83}$$

is the mean length of one turn of the stator winding per phase and $l_{ce}$ is the length of end connection given by

$$l_{ce} = \theta_p \tau / 180^{\circ} \tag{84}$$

$X_1$ represent the inductance per phase :

$$X_1 = \frac{2\mu_0 \pi f \left[ \left( \lambda_s \left( 1 + \frac{3}{p} \right) + \lambda_d \right) \frac{W_s}{q_1} + \lambda_e l_{ce} \right] N_1^2}{p} \tag{85}$$

where

$$\lambda_s = h_s(1 + 3k_p)/12w_s \tag{86}$$

$$\lambda_e = 0.3(3k_p - 1) \tag{87}$$

and

$$\lambda_d = \frac{5(ge/ws)}{5 + 4g_0/w_s} \tag{88}$$

Transverse End Effect Parameters are implemented based on the study done in [21]

$$C_r = \frac{sG\big([Re(T)]^2 + [Im(T)]^2\big)}{Re(T)} \tag{89}$$

$$C_x = \frac{\big([Re(T)]^2 + [Im(T)]^2\big)}{Im(T)} \tag{90}$$

$$T = j\big[\gamma^2 + (1 - \gamma^2)\frac{\xi}{a\eta} th(a\eta)\big] \tag{91}$$

$$\gamma = \sqrt{\frac{1}{1 + jsG}} \tag{92}$$

$$\xi = \left[ 1 + \frac{1}{\gamma} th(a\eta) th(\frac{\pi}{\tau}(\tau - a)) \right]^{-1} \tag{93}$$

# Chapter 9
# Parameters Effecting on a short secondary Double Sided Linear Induction Motors

Due to that fact that our motor will be used in haptic interface application the frequency will range between 70 Hz to 700 Hz, the velocity of the secondary will vary between 0 and 0.1 m/s and the angle Theta will go from zero to $\pi/12$ . The goal of this study is to know how to identify our system due to uncertainty on our parameters only based on parameters that effect our System in significant way.Although The slip is semi-static but a general study of slip effect have also been done.

## 9.1 Frequency Effect

Based on MATLAB simulation the force will decrease while we increase the frequency.

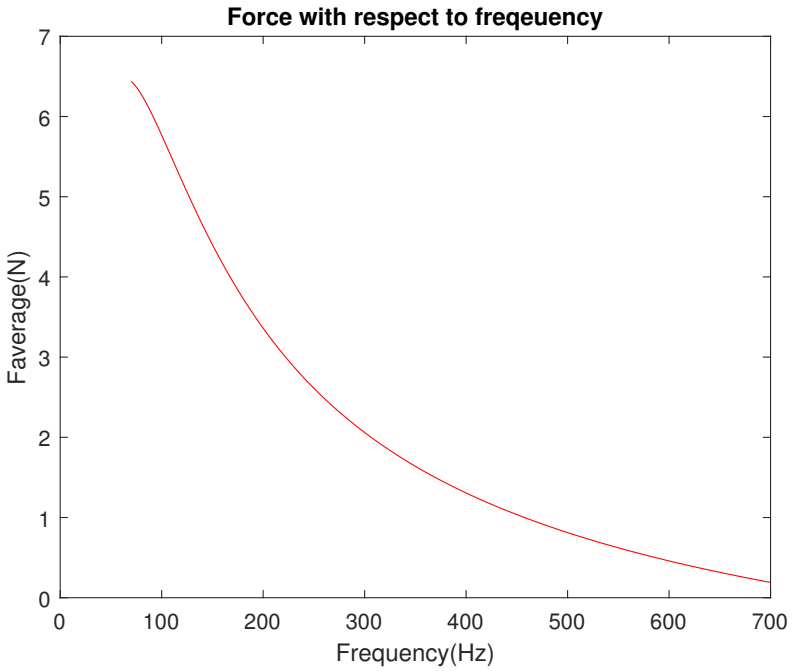


Figure 27: Force vs Frequency

## 9.2 Secondary Velocity Effect

In order to understand the effect of the secondary velocity .A ratio of maximum force over minimum force with respect to a velocity varying from 0 to 0.1 m/s will be represent it on each frequency.

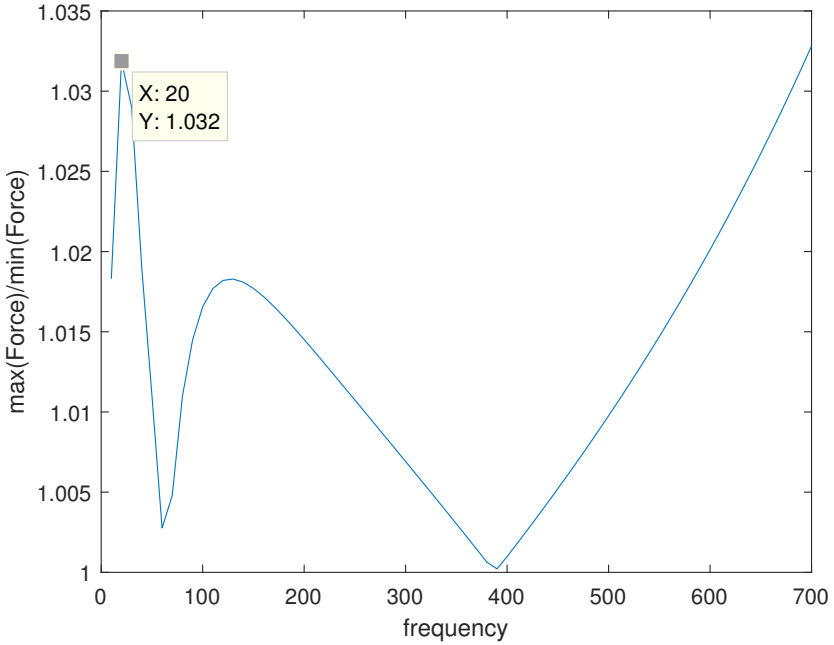


Figure 28: Max(Force)/Min(Force) with respect to frequency

We can notice that the ratio is varying between 1 and 1.033.Which is negligible .So Velocity will not be taken in identifying our system.It will be considered constant equal to zero.

## 9.3 Orientation effect

Based on Figure 24 ,a simulation is done to understand the effect of angle $\theta$ on force generation.The figure below will show us the increase of force with respect to angle due to the fact that common surface between the primary and secondary will increase.

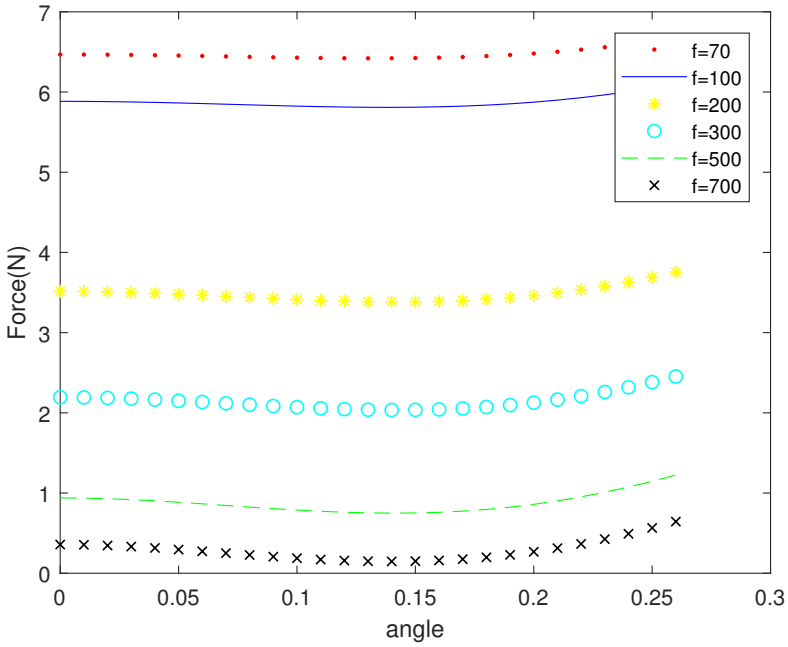


Figure 29: Force with respect to angle for different frequency

We can notice that orientation effect decrease with respect to frequency due to high value of force so sensitivity with respect to angle decrease.

## 9.4 Slip effect

We care about the slip range 0.9-1 because our velocity is always low so the slip value will be almost equal to 1. The graph below represent the variation of force with respect to slip value.We notice the effect of slip increasing on force differ depending on the case .High frequency case:the force value decrease.Low frequency case the force will increase.

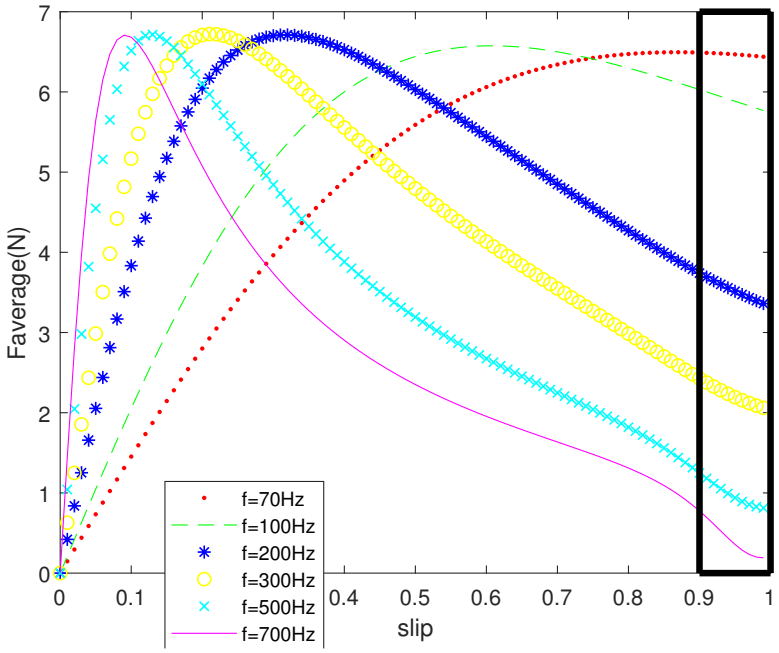


Figure 30: Force with respect to slip for different value of frequency

# Chapter 10
# System Identification

The non-linear motor transfer function is described by a Hammerstein model.Where y(t) is the generated force and u(t) is the input frequency.

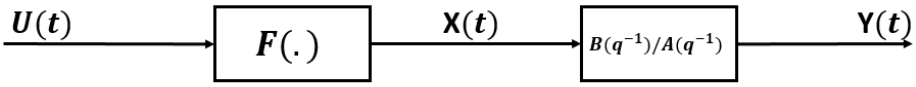


Figure 31: Hammerstein model

In order to generate input signal Maxon brushless motor controller is used which is a six step voltage source as an input.

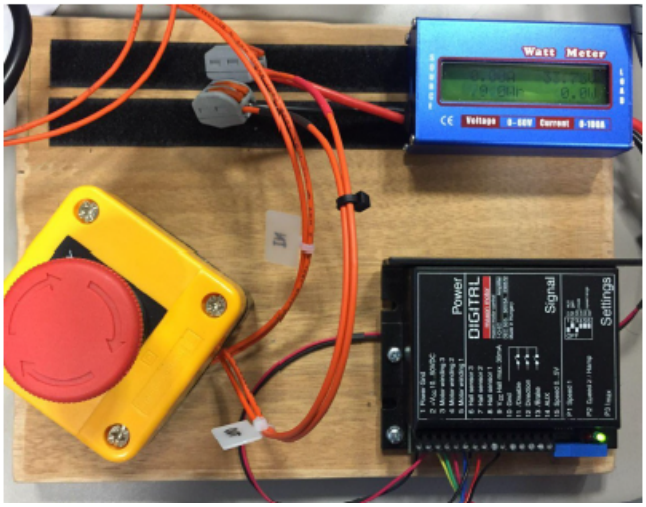


Figure 32: Maxon brushless motor controller

## 10.1 Steady state System Identification

Based on our equivalent circuit and parameters effect:
We collect data about our system so we went from black box system Identification problem into semi-black box Problem.
After solving system equations and simulating them on MATLAB, we got results about the effectiveness of parameters(i.e velocity effect,...) for further details see section 9 .

The generated force by our system is modulated by:

$$F_x(f,\theta,I) = K(f,\theta)I^2 \tag{94}$$

Or

$$F_x(f,\theta,U) = K^{'}(f,\theta)U^2 \tag{95}$$

The only modeling difference between the two representation is related to control method(i.e using current stabilizer in the controller design 94 or without using it95 . A data should be collected from experiments so we can identify our system.Using NI chip ,we collect Force,potential difference,frequency in order to estimate $K^{'}$ same procedure for K but collecting I instead of U.
A rotary motor equation is simple and easy to estimate due to the fact that Xm is constant.On the other side,linear induction motor magnetizing value is variable.Another difference between these motors is the distribution of magnetic field along the x axis;In a rotary motor the magnetic field is sinusoidal which is an harmonic function of order 2 in linear induction motor .Due to those reasons a normal system Identification method is not efficient.
Based on power equation ,we can reformulate force equation. Which will lead us into a better representation of K or K'.

$$K = \frac{K_1 K_2 f}{(1 + k_2^2 f^2)cos\theta} \tag{96}$$

or

$$K^{'} = \frac{K_1^{'} K_2^{'} f}{(1 + k_2^{'2} f^2)cos\theta} \tag{97}$$

Our system Identification method will be least square method.
Due to longitudinal and transverse end effect, a second losses term should be added to represent them.

$$LossesTerm = \frac{(af^3 + bf^2 + cf + d)}{ef^4 + gf^3 + hf^2 + if + k} I^2 \tag{98}$$

or

$$LossesTerm = \frac{(a'f^3 + b'f^2 + c'f + d')}{e'f^4 + g'f^3 + h'f^2 + i'f + k'} U^2 \tag{99}$$

In order to reduce the losses term complexity,we noticed experimentally and theoretically a variation in the shape of the force plot after certain frequency.Therefore,system Identification was done on two range which leads to get two function each one in a range.In order to link those function,sigmoid function was used.

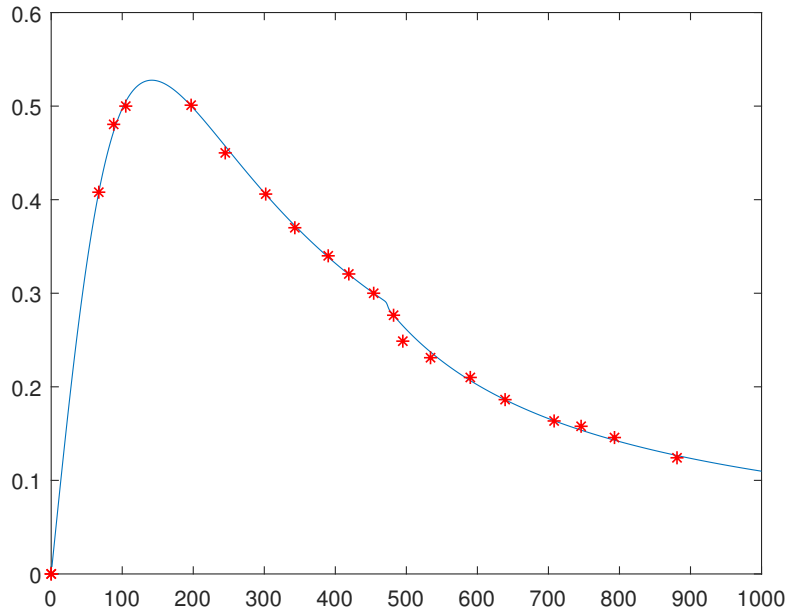


Figure 33: Estimated Vs Experimental results

## 10.2 Linear Block Identification

After testing several data from motor simulation we can notice that the best fit was estimated base on a transfer function with zero or one zero and 3 poles.Starting from this assumption a random variable frequency signal input will be generated so we can estimate X in order to find the dynamical block(Linear Block). As a result of simulation we noticed that 1 zeros and 3 poles showed better fit result then 1 zero with 3 poles with a fit of 60%.

$$G(q^{-1}) = \frac{B(q^{-1})}{A(q^{-}1)} = \frac{147.155s + 1.2609 \times 10^4}{s^3 + 43.3525s^2 + 1185s + 1.2609 \times 10^4} \tag{100}$$

Due to the fact that input signal is not sinusoidal and dynamics of the Maxon brushless motor controller the systemIdetification is not precise and contains a lot of uncertainty in order to be precise a system Identification have been done on the motor by generating a random frequency and getting the frequency in order to identify it using Hammerstein-Weiner model .

## 10.3 Hammerstein-Weiner model

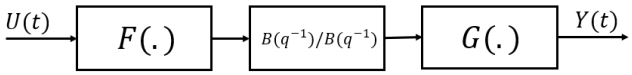


Figure 34: Hammerstein-Weiner Model

Using this type of model we were able to cover all type of uncertainty and non-linearity due to the control circuit and nonlinear signal generation.
Input non-linearity and Output non-linearity are covered by a polynomial of order 10 while the linear block is a bock of order 3. By comparing this model to data generated by random input signal we got a fit of 91.58 % and a maximum absolute error of 0.008 .

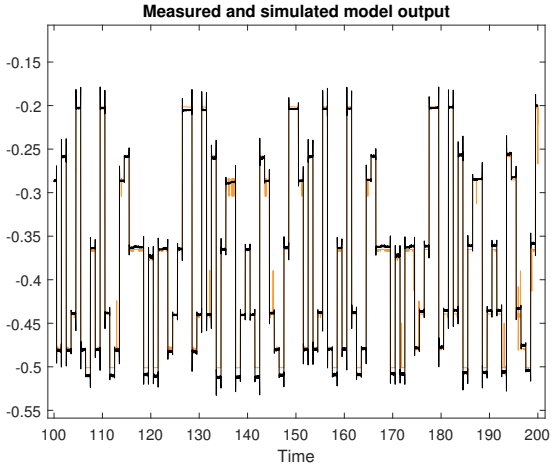


Figure 35: Simulation Vs Measured data

# Chapter 11
# MATLAB Simulink

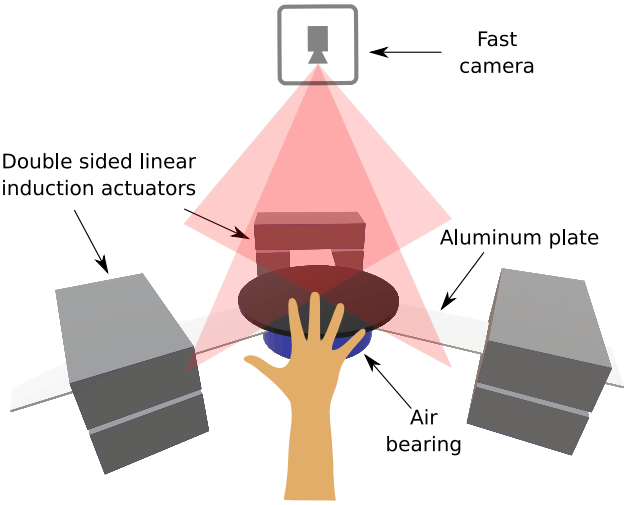


Figure 36: Planar Haptic Interface, based on Double Sided Linear Induction Actuators

The Aim of this motor is to be applied on haptic interface device. Based on force equation of motors ,Newton's law and Euler Law. We can study the motion of haptic handle using equation described and simulink tools in order to simulate our differential equations.

## 11.1 Differential equations

Derived from Newton and Euler Equations:

$$\begin{aligned} \sum Fx_i &= m\ddot{x} \\ \sum Fy_i &= m\ddot{y} \\ \sum M_z &= I\ddot{\theta} \end{aligned} \tag{101}$$

we get:

$$\begin{aligned} &Fx_{uppermotor} - F_{right}cos(\pi/3) + F_{left}cos(\pi/3) + Fx_{human} = m\ddot{x} \\ &- F_{right}sin(\pi/3) + F_{left}sin(\pi/3) + Fy_{human} = m\ddot{y} \\ &(\gamma + a)(Fx_{uppermotor} + F_{right} + F_{left}) = I\ddot{\theta} \end{aligned} \tag{102}$$

## 11.2 Simulink Blocks

In order to generate linear induction motor force a generating force block will be used with an input frequency ,voltage supply and haptic handle orientation. In the figure below an image of simulink block of the upper motor used.Two other blocks are used to present the motors on the right and left of the haptic handle.

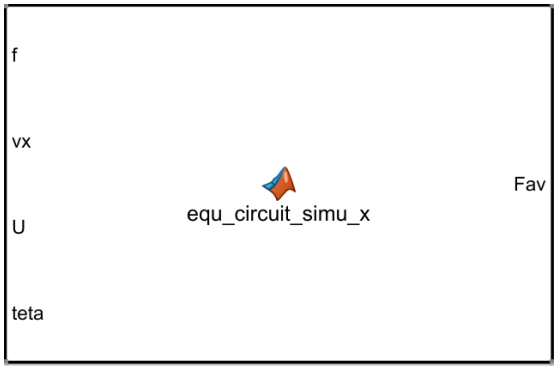


Figure 37: Linear Induction Motor block

Another block will represent Euler and Newton equation. Human force and torque will be also taken into consideration in our system. In the figure below ,a representation of the LIM motors forces and Newton-Euler equations.

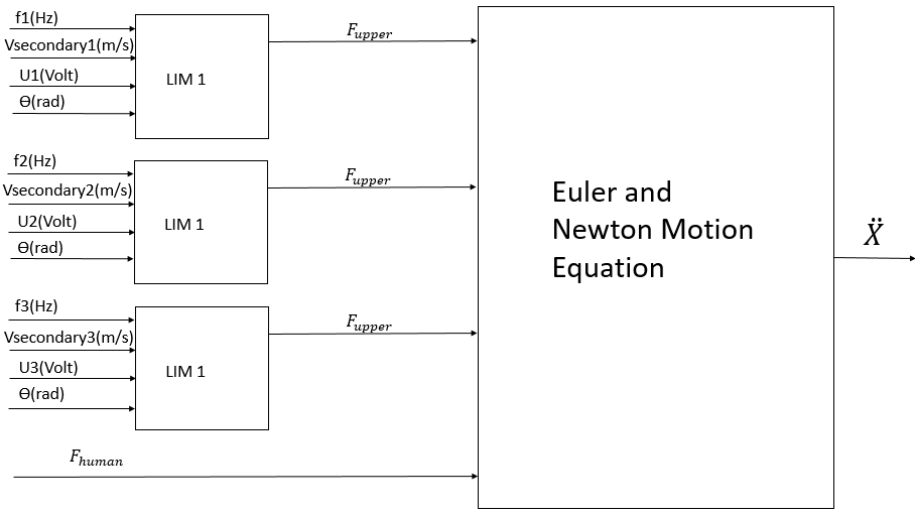


Figure 38: System model

# Chapter 12
# Conclusion and Future Improvements

As a conclusion ,We should change the motor parameters with a shift between the primary plate in order to get a sinusoidal magnetic filed which will lead to a force without vibrations.Deep study into motors inputs lead to a minimization of those input to be taken into consideration in the system Identification .The system Identification of the motor pushed the research into future improvement step by modeling the motor in order to be used in the design of the controller that will push us further in getting a high fidelity haptic interface .

## References


[1] R. S. Fearing, "Survey of sticking effects for micro parts handling," vol. 2, pp. 212–217 vol.2, Aug 1995.

[2] A. Bolopion and S. Régnier, "A review of haptic feedback teleoperation systems for micromanipulation and microassembly," IEEE Transactions on Automation Science and Engineering, vol. 10, pp. 496–502, July 2013.

[3] F. Beyeler, S.Muntwyler, Z. Nagy, C. Graetzel,M.Moser, and B. J. Nelson, "Design and calibration of a mems sensor for measuring the force and torque acting on a magnetic microrobot," Journal of Micromechanics and Microengineering, vol. 18, no. 2, p. 025004, 2008.

[4] A. Bolopion, H. Xie, D. S. Haliyo, and S. Regnier, "Haptic teleoperation for 3-d microassembly of spherical objects," IEEE/ASME Transactions on Mechatronics, vol. 17, pp. 116–127, Feb 2012.

[5] A. Ferreira and C. Mavroidis, "Virtual reality and haptics for nanorobotics," IEEE Robotics AutomationMagazine, vol. 13, pp. 78–92, Sept 2006.

[6] I. Bukusoglu, C. Basdogan, A. Kiraz, and A. Kurt, "Haptic manipulation of microspheres using optical tweezers under the guidance of artificial force fields," Presence: Teleoperators and Virtual Environments, vol. 17, no. 4, pp. 344–364, 2008.

[7] S. J. Bolanowski, G. A. Gescheider, R. T. Verrillo, and C.M. Checkosky, "Four channels mediate the mechanical aspects of touch.," The Journal of the Acoustical Society of America, vol. 84 5, pp. 1680–94, 1988.

[8] F. A. Geldard, "Some neglected possibilities of communication," Science (New York, N.Y.), vol. 131, pp. 1583–8, 06 1960.

[9] V. Hayward, O. R. Astley, M. Cruz-Hernandez, D. Grant, and G. Robles-De-La-Torre, "Haptic interfaces and devices," Sensor Review, vol. 24, no. 1, pp. 16–29, 2004.

[10] J. C. Craig and G. B. Rollman, "Somesthesis," Annual Review of Psychology, vol. 50, no. 1, pp. 305–331, 1999. PMID: 10074681.

[11] V. Perez and M. Santís-Chaves, " HAPTIC INTERFACES: KINESTHETIC VS. TACTILE SYSTEMS," Revista EIA, pp. 13 – 29, 12 2016.

[12] C. Hatzfeld, Haptics as an Interaction Modality, pp. 29–100. London: Springer London, 2014.

[13] R. T. Verrillo, "Effect of contactor area on the vibrotactile thresold," Journal of The Acoustical Society of America - J ACOUST SOC AMER, vol. 35, 12 1963.

[14] F. Clark, P. Grigg, and J. Chapin, "The contribution of articular receptors to proprioception with the fingers in humans," Journal of Neurophysiology, vol. 61, no. 1, pp. 186–193, 1989.

[15] T. Zeng, F. Giraud, B. Lemaire-Semail, and M. Amberg, "Analysis of a new haptic display coupling tactile and kinesthetic feedback to render texture and shape," in Haptics: Generating and Perceiving Tangible Sensations (A.M. L. Kappers, J. B. F. van Erp, W. M. Bergmann Tiest, and F. C. T. van der Helm, eds.), (Berlin, Heidelberg), pp. 87– 93, Springer Berlin Heidelberg, 2010.

[16] K. Sato, H. Kajimoto, N. Kawakami, and S. Tachi, "Electrotactile display for integration with kinesthetic display," in RO-MAN 2007 - The 16th IEEE International Symposium on Robot and Human Interactive Communication, pp. 3–8, Aug 2007.

[17] M. Fritschi, M. Ernst, and M. Buss, "Integration of kinesthetic and tactile display - a modular design concept," 01 2006.

[18] M. Y. Tsalamlal, N. Ouarti, and M. Ammi, "Non-intrusive haptic interfaces: State-ofthe art survey," in Haptic and Audio Interaction Design (I. Oakley and S. Brewster, eds.), (Berlin, Heidelberg), pp. 1–9, Springer Berlin Heidelberg, 2013.

[19] G. Millet, S. Haliyo, S. Regnier, and V. Hayward, "The ultimate haptic device: First step," in World Haptics 2009 - Third Joint EuroHaptics conference and Symposium on Haptic Interfaces for Virtual Environment and Teleoperator Systems, pp. 273–278, March 2009.

[20] V. Hayward and K. E.Maclean, "Do it yourself haptics: part i," IEEE Robotics AutomationMagazine, vol. 14, pp. 88–104, Dec 2007.

[21] YANG TZHOU L BLI L R Performance calculation for double sided linear induction motor with short secondaryC/ / International Conference on Electrical Machines and SystemsOctober 17 202008WuhanChina3478 3483